Available online at www.sciencedirect.com
SCIENCE DIRECT®
ELSEVIER
International Journal of Solids and Structures 43 (2006) 2126–2145
INTERNATIONAL JOURNAL OF SOLIDS and STRUCTURES
www.elsevier.com/locate/ijsolstr

Crack spacing effect for a piezoelectric cylinder under electro-mechanical loading or transient heating

Jie-Cai Han, Bao-Lin Wang *

Graduate School at Shenzhen, Harbin Institute of Technology, Harbin 150001, P.R. China

Received 16 December 2004; received in revised form 27 June 2005
Available online 25 August 2005

Abstract

This paper investigates the fracture problem of a piezoelectric cylinder with a periodic array of embedded circular cracks. An electro-mechanical fracture mechanics model is established first. The model is further used to the thermal fracture analysis of a piezoelectric cylinder subjected to a sudden heating on its outer surface. The temperature field and the associated thermal stresses and electric displacements are obtained and are added to the crack surface to form a mixed-mode boundary value problem for the electro-mechanical coupling fracture. The stress and stress intensities are investigated for the effect of crack spacing. Strength evaluation of piezoelectric materials under the transient thermal environment is made and thermal shock resistance of the medium is given.

Keywords: Thermal stresses; Fracture mechanics; Piezoelectric materials

1. Introduction

Since piezoelectric materials are very brittle and susceptible to fracture, it is necessary to understand the fracture behaviors of these advanced materials. On the other hand, mechanical, electrical, and thermal fields are coupled in most physical problems. Thermal effects in piezoelectric materials could be important when those materials are used at high or low temperature environments. In a series of their work, Herrmann and Loboda investigated interface cracks with a frictionless contact zone at the crack tip between two semi-infinite piezoelectric spaces under the action of a remote electro-mechanical loading and a temperature flux (Herrmann and Loboda, 2003a,b). Gao et al. (2002) presented an exact solution

* Corresponding author. Address: Harbin Institute of Technology, Center for Composite Materials, Harbin 150001, China. Tel.: +86 755 260 33490; fax: +86 755 260 33491.
E-mail address: wangbl2001@hotmail.com (B.-L. Wang).

0020-7683/$ - see front matter © 2005 Elsevier Ltd. All rights reserved.
doi:10.1016/j.ijsolstr.2005.06.080

for the problem of an elliptic hole or a crack in a thermopiezoelectric solid. The method used in that paper was also applied to an elliptical cavity in a magnetoelectroelastic solid under remotely uniform in-plane electromagnetic and/or anti-plane mechanical loading (Gao et al., 2004). The thermoelastic behavior of piezoelectric solids with defects, such as holes and interface cracks, were considered by Zhang et al. (2002), and by Qin and Mai (1999). The problem of a 2-D piezoelectric material with an elliptic cavity under uniform heat flow was investigated by Lu et al. (1998). Studied by Niraula and Noda (2002) was a transversely isotropic thermopiezoelastic material strip containing an edge crack under thermal and electrical loading conditions. Recently, the thermally induced fracture problem for a piezoelectric laminate with a crack subject to uniform electric and temperature fields was considered by Ueda (2003). A surface crack in a piezoelectric strip under transient thermal load was investigated by Wang and Mai (2003). The exact solution for a penny-shaped crack in a piezoelectric medium under steady thermal flux was given by Wang and Noda (2004). Shang et al. (2003) investigated propagation behavior of an elliptical crack in thermopiezoelectric material subjected to a uniform temperature. The three-dimensional strain energy density formulation was used to determine the direction of crack propagation and the shape of the initial fracture increment. Gu and Yu (2003) considered the anti-plane problem of thermal effect near crack tip region of piezoelectric material subjected to electrical impact loading by means of the integral transforms and the singular integral equations.

Although a variety of challenging issues related to certain thermal crack problems in the piezoelectric materials have been addressed, one of the remaining problems that need to be fully understood is that of a periodic array of parallel cracks in such media subjected to thermal loading. Past experience suggests that cracks in a medium may be either a single dominant crack or a roughly regular array of periodic cracks (Grot and Martyn, 1981; Rizk, 2004; Timm et al., 2003; Erdogan and Ozturk, 1995; Ishihara and Noda, 2001). Therefore, it is important to consider multiple cracking of piezoelectric media.

This paper investigates the thermal fracture of a piezoelectric cylinder with a periodic array of embedded circular cracks. Both electro-mechanical loads and thermal loads are considered. The crack problem is solved by means of integral equation technique. Effect of crack spacing on the stress and crack front field intensity factors are investigated. The thermal shock (transient thermal loading) resistance of a piezoelectric material is studied for a cylinder specimen subjected to a sudden heating on its outer surface. Some conclusions are drawn.

2. Electro-mechanical model for a row of infinitesimal periodic cracks

This section develops an electro-mechanical model for a periodic array of cracks in a piezoelectric cylinder (Fig. 1). The analytical model is generalized for any distribution of the electro-mechanical loads on the crack faces. The cylindrical coordinates r, θ and z are coincident with the principal axes of the material symmetry. We investigate an axis-symmetric problem such that all the field variables are functions of the radial coordinate r and the axial coordinate z only. Hereafter θ denotes the circumferential coordinate; the symbols and D denote the stress and electric displacement, respectively; u and w are, respectively, the radial and axial components of the displacement vector; and ϕ is the electric potential. Constitutive equations for piezoelectric materials whose poling direction is coincident with the positive z-axis are (Lin et al., 2003):

$$\sigma_{rr} = c_{11}\frac{\partial u}{\partial r} + c_{12}\frac{u}{r} + c_{13}\frac{\partial w}{\partial z} + e_{31}\frac{\partial \phi}{\partial z} - \lambda_{11}T, \tag{1a}$$

$$\sigma_{\theta\theta} = c_{12}\frac{\partial u}{\partial r} + c_{11}\frac{u}{r} + c_{13}\frac{\partial w}{\partial z} + e_{31}\frac{\partial \phi}{\partial z} - \lambda_{11}T, \tag{1b}$$

$$\sigma_{zz} = c_{13}\frac{\partial u}{\partial r} + c_{13}\frac{u}{r} + c_{33}\frac{\partial w}{\partial z} + e_{33}\frac{\partial \phi}{\partial z} - \lambda_{33}T, \tag{1c}$$

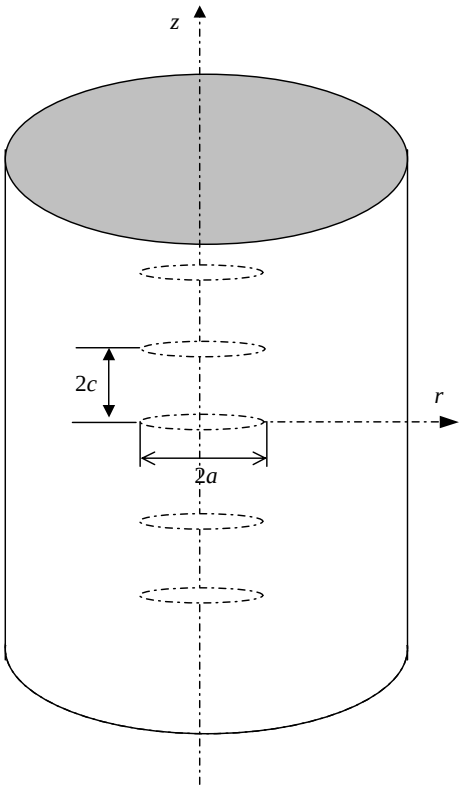

Fig. 1. A periodic array of embedded circular cracks in a piezoelectric medium ($2c$: crack spacing; a: crack radius).

$$\sigma_{rz} = c_{44}\left(\frac{\partial u}{\partial z} + \frac{\partial w}{\partial r}\right) + e_{15}\frac{\partial \phi}{\partial r}, \tag{1d}$$

$$D_r = e_{15}\left(\frac{\partial u}{\partial z} + \frac{\partial w}{\partial r}\right) - \epsilon_{11}\frac{\partial \phi}{\partial r}, \tag{1e}$$

$$D_z = e_{31}\frac{\partial u}{\partial r} + e_{31}\frac{u}{r} + e_{33}\frac{\partial w}{\partial z} - \epsilon_{33}\frac{\partial \phi}{\partial z} - \beta_3 T, \tag{1f}$$

where c_{ij}, e_{ij} and ϵ_{ii} are elastic constants, piezoelectric constants and dielectric permittivities, respectively; λ_{ii} are the temperature–stress coefficients; β_3 is the temperature–electric displacement coefficient; T is the temperature change in the medium.

In the absence of body forces and body charges, the equilibrium equations for the piezoelectric media are (Lin et al., 2003):

$$\frac{\partial \sigma_{rr}}{\partial r} + \frac{\partial \sigma_{rz}}{\partial z} + \frac{\sigma_{rr} - \sigma_{\theta\theta}}{r} = 0, \tag{2a}$$

$$\frac{\partial \sigma_{rz}}{\partial r} + \frac{\partial \sigma_{zz}}{\partial z} + \frac{\sigma_{rz}}{r} = 0, \tag{2b}$$

$$\frac{\partial D_r}{\partial r} + \frac{\partial D_z}{\partial z} + \frac{D_r}{r} = 0, \tag{2c}$$

which can be expressed in terms of displacements and electric potential with substitution of the constitutive Eq. (1). The system governing Eqs. (1) and (2) must be solved under prescribed electro-mechanical boundary conditions.

2.1. Electro-mechanical boundary conditions

Generally, the crack surfaces are traction free. However, because the air or vacuum allows some penetration of electric flux through the crack interior, the electric displacement inside the crack may not be zero and it's normal component (along the z direction) is denoted as d_0. Then, the mixed boundary conditions on the $z = 0$ plane can be stated as follows:

$$\sigma_{zz}(r,0) = p_{01}(r) = -\sigma_0(r), \quad D_z(r,0) = p_{02}(r) = d_0(r) - D_0(r), \qquad r < a, \tag{3a}$$

$$w(r,0) = 0, \quad \phi(r,0) = 0, \qquad r \geqslant a, \tag{3b}$$

where $\sigma_0(r)$ and $D_0(r)$ are the values obtained from the solution without any cracks. Because of symmetry and periodicity, the problem can be considered for an infinite disk $-c < z < c$, subjected to the following homogeneous boundary conditions:

$$\sigma_{rz}(r,-c) = \sigma_{rz}(r,0) = \sigma_{rz}(r,c) = 0, \tag{4}$$

$$w(r,-c) = w(r,c) = 0, \tag{5a}$$

$$\phi(r,-c) = \phi(r,c) = 0. \tag{5b}$$

The solution of the disk is obtained in terms of some unknown coefficients. These unknown coefficients are then determined from the boundary conditions of the problem through the introduction of a displacement and electric potential discontinuity function vector along the cracked plane (i.e. the $z = 0$ plane).

2.2. Electro-mechanical fields in the piezoelectric medium

Referring to the constitutive relations and the equilibrium equations for the piezoelectric medium poled along the positive z-axis (Eqs. (1) and (2)), the displacements and electric potential can be expressed as

$$\begin{Bmatrix} u(r,z) \\ w(r,z) \\ \phi(r,z) \end{Bmatrix} = \int_0^\infty \sum_{m=1}^{6} \begin{Bmatrix} a_{1m}J_1(sr) \\ a_{2m}J_0(sr) \\ a_{3m}J_0(sr) \end{Bmatrix} \exp(s\lambda_m z) A_m \, \mathrm{d}s, \tag{6}$$

where J_i $(i = 0, 1)$ are the ith order Bessel functions of the first kind, $A_m(s)$ are unknown functions of s, and the constants a_{1m}, a_{2m}, a_{3m}, and the parameter λ are determined from

$$\begin{bmatrix} c_{11} - c_{44}\lambda_m^2 & (c_{13} + c_{44})\lambda_m & (e_{31} + e_{15})\lambda_m \\ (c_{13} + c_{44})\lambda_m & c_{33}\lambda_m^2 - c_{44} & e_{33}\lambda_m^2 - e_{15} \\ (e_{31} + e_{15})\lambda_m & e_{33}\lambda_m^2 - e_{15} & \epsilon_{11} - \epsilon_{33}\lambda_m^2 \end{bmatrix} \begin{Bmatrix} a_{1m} \\ a_{2m} \\ a_{3m} \end{Bmatrix} = 0. \tag{7}$$

Eq. (7) is an eigenvalue problem consisting of three equations. Nontrivial a_{jm} $(j = 1, 2, 3)$ exist if λ is a root of the determinant. In Eq. (7), there are six roots for λ_m. It can be shown that if $[\lambda_m, (a_{1m}, a_{2m}, a_{3m})^{\mathrm{T}}]$ is an eigensolution, then $[-\lambda_m, (a_{1m}, -a_{2m}, -a_{3m})^{\mathrm{T}}]$ is also an eigensolution, of Eq. (7).

In what follows, the order of the roots λ_m are arranged such that $\mathrm{Re}(\lambda_1) < 0$, $\mathrm{Re}(\lambda_2) < 0$, $\mathrm{Re}(\lambda_3) < 0$ and $\lambda_4 = -\lambda_1$, $\lambda_5 = -\lambda_2$, $\lambda_6 = -\lambda_3$. Substituting Eq. (6) into the constitutive equations, the stresses and electric displacements can be obtained as

$$\begin{Bmatrix} \sigma_{zz}(r,z) \\ D_z(r,z) \\ \sigma_{zr}(r,z) \end{Bmatrix} = \sum_{m=1}^{6} \int_0^\infty s \begin{Bmatrix} C_{1m}J_0(sr) \\ C_{2m}J_0(sr) \\ C_{3m}J_1(sr) \end{Bmatrix} \exp(s\lambda_m z) A_m \, \mathrm{d}s, \tag{8a}$$

$$\sigma_{rr}(r,z) = \sum_{m=1}^{6} \int_0^\infty \left[C_{4m}sJ_0(sr) + \frac{c_{12}-c_{11}}{r} a_{1m}J_1(sr) \right] \exp(s\lambda_m z) A_m \, \mathrm{d}s, \tag{8b}$$

$$D_r(r,z) = \sum_{m=1}^{6} C_{5m} \int_0^\infty sJ_1(sr) \exp(s\lambda_m z) A_m \, \mathrm{d}s, \tag{8c}$$

where the constants C_{jm} ($j = 1,\ldots,5$; $m = 1,2,3$) are given in Appendix A.

The unknown coefficients A_m will be determined from the symmetry and periodicity conditions (4) and (5), as well as the mixed-mode conditions (3). This will be done by introducing an auxiliary function vector on the cracked plane.

2.3. Satisfying the symmetry and periodicity conditions

In order to consider the mixed-mode boundary conditions (3) on the cracked plane, an auxiliary vector $g = (g_1, g_2)^{\mathrm{T}}$ is defined in the following manner:

$$g_1(s) = \sum_{m=1}^{3} A_m a_{2m}, \qquad g_2(s) = \sum_{m=1}^{3} A_m a_{3m}. \tag{9}$$

It follows from the symmetry condition (4), periodicity conditions (5), and with substitution of Eq. (6) into Eq. (9), A_m can be expressed in terms of the displacement discontinuity function g as

$$A_m(s) = \sum_{j=1}^{2} b_{mj}(s) g_j(s), \tag{10}$$

where b_{mj}, ($m = 1,\ldots,6$; $j = 1,2$) are known coefficients:

$$b_{mj} = \frac{1}{1 - \exp(2sc\lambda_m)} B_{mj}, \quad b_{(m+3)j} = \exp(2sc\lambda_m) b_{mj} \quad (m = 1,2,3), \tag{11}$$

in which B_{mj} are the elements of the following matrix:

$$[B] = \begin{bmatrix} a_{21} & a_{22} & a_{23} \\ a_{31} & a_{32} & a_{33} \\ C_{31} & C_{32} & C_{33} \end{bmatrix}^{-1}. \tag{12}$$

Now considering the boundary conditions (3b), it follows that

$$\int_0^\infty g_j(s) J_0(sr) \, \mathrm{d}s = 0 \quad (j = 1,2) \;\; r \geqslant a. \tag{13}$$

Hence, g_i ($i = 1,2$) have the solutions of the form

$$g_j(s) = \int_0^a \Phi_j(l) \sin(sl) \, \mathrm{d}l \quad (j = 1,2), \tag{14}$$

provided that $\lim_{t\to 0} \Phi_j(t) = 0$. The functions $\Phi_j(r)$ will be determined from the crack face boundary conditions through a system of Fredholm integral equations of the second kind.

2.4. The integral equations

The system of integral equations can be obtained by substituting Eqs. (10) and (14) into Eq. (8a), and using crack face boundary conditions (3a). It can be shown that

$$\int_0^\infty J_0(sx)\left[\int_0^a s\sin(sl)\sum_{j=1}^{2}\Lambda_{ij}(s)\Phi_j(l)\,\mathrm{d}l\right]\mathrm{d}s = p_{0i}(x) \quad (i=1,2). \tag{15}$$

The contractions

$$\Lambda_{ij}(s) = \sum_{m=1}^{6} C_{im}b_{mj}(s) \quad (i,j=1,2), \tag{16}$$

have been made. In order to determine the possible singular behavior of Eq. (15), the behavior of the kernel $[\Lambda]$ for large value of s needs to be examined. It can be seen from Eq. (11) that as s approaches infinity, the quantities $b_{4j}(s)$, $b_{5j}(s)$ and $b_{6j}(s)$ are zero, and $b_{1j}(s)$, $b_{2j}(s)$ and $b_{3j}(s)$ are constants: $b_{mj}(s=\infty)=B_{mj}$, in which $(m=1,2,3)$ and $(j=1,2)$. By adding and subtracting the asymptotic values $b_{mj}(\infty)$ to and from $b_{mj}(s)$ in Eq. (16), Eq. (15) can be re-written as

$$\int_0^\infty J_0(sx)\left[\int_0^a s\sin(sl)\sum_{j=1}^{2}\Lambda^0_{ij}\Phi_j(l)\,\mathrm{d}l\right]\mathrm{d}s + \int_0^a \psi_{ij}(x,r)\Phi_j(r)\,\mathrm{d}r = p_{0i}(x), \tag{17}$$

where $(i=1,2)$, Λ^0_{ij} are material constants:

$$\Lambda^0_{ij} = \sum_{m=1}^{3} C_{im}B_{mj} \tag{18}$$

and ψ_{ij} are functions of x and r:

$$\psi_{ij}(x,r) = \sum_{m=1}^{3} C_{im}B_{mj}\int_0^\infty J_0(sx)\frac{2s\exp(2sc\lambda_m)}{1-\exp(2sc\lambda_m)}\sin(sr)\,\mathrm{d}s. \tag{19}$$

For $c\to\infty$ (infinite crack spacing) or $r\to y$, the above Eq. (19) gives $\psi_{ij}=0$. Accordingly, integral Eq. (17) reduce to the single crack solution when c approaches infinity.

Referring to Appendix B for details, the integral Eq. (17) can be further simplified to

$$\sum_{j=1}^{2}\left[\Lambda^0_{ij}\Phi_j(l) + \int_0^a K_{ij}(l,r)\Phi_j(r)\,\mathrm{d}r\right] = Q_i(l), \tag{20}$$

where $(i=1,2)$, and the integral kernels K_{ij} and the generalized loads Q_i are

$$K_{ij}(l,r) = \frac{4}{\pi}\sum_{m=1}^{3} C_{im}B_{mj}\int_0^\infty \frac{\exp(2sc\lambda_m)}{1-\exp(2sc\lambda_m)}\sin(sr)\sin(sl)\,\mathrm{d}s \tag{21}$$

and

$$Q_i(l) = \frac{2}{\pi}\int_0^l \frac{xp_{0i}(x)}{\sqrt{l^2-x^2}}\,\mathrm{d}x, \tag{22}$$

respectively.

2.4.1. Stress and electric displacement intensity factors

Eq. (20) is the desired system of integral equations which can be solved by a standard method (e.g. by collocation technique). Since Eq. (22) contains an unknown constant d_0, which is the normal component of the electric displacement vector inside the crack (see Eq. (3a)). To obtain d_0 and Φ_j $(j = 1, 2)$ from Eq. (20), an additional assumption is needed. This will be discussed in the following Section 2.5. Once d_0 and Φ_j $(j = 1, 2)$ are known, the full-field solution is obtained. From the expressions

$$k_1 = \lim_{r\to a} \sqrt{2(x-a)}\sigma_{zz}(r,0), \qquad k_{\mathrm{D}} = \lim_{r\to a} \sqrt{2(x-a)}D_z(r,0), \tag{23}$$

the stress and electric displacement intensity factors are obtained as

$$k_1 = -\frac{1}{\sqrt{a}}\sum_{j=1}^{2} \Lambda_{1j}\Phi_j(a), \qquad k_{\mathrm{D}} = -\frac{1}{\sqrt{a}}\sum_{j=1}^{2} \Lambda_{2j}\Phi_j(a). \tag{24}$$

The normal displacement and electric potential on the upper surface of the crack can be determined from Eqs. (6), (10) and (14), which are

$$\left\{ \begin{array}{c} w(r,0) \\ \phi(r,0) \end{array} \right\} = \int_r^a \frac{1}{\sqrt{t^2 - r^2}} \left\{ \begin{array}{c} \Phi_1(t) \\ \Phi_2(t) \end{array} \right\} \mathrm{d}t. \tag{25}$$

2.4.2. Stress and electric displacement

Two quantities of considerable practical interest are the stress $\sigma_{zz}(r,z)$ and the electric displacement $D_z(r,z)$, as it may have a bearing on further cracking on cell division. It is expected that the overall stress is maximized at the plane $z = c$ (Erdogan and Ozturk, 1995; Schulze et al., 1998). Substituting Eqs. (10) and (14) into Eq. (8a), the stress and electric displacement at the plane $z = c$ can be obtained as follows:

$$\left\{ \begin{array}{c} \sigma_{zz}(r,c) \\ D_z(r,c) \end{array} \right\} = 2\sum_{m=1}^{3} \left\{ \begin{array}{c} C_{1m} \\ C_{2m} \end{array} \right\} \int_0^a R_m(r,l) \sum_{j=1}^{2} B_{mj}\Phi_j(l)\,\mathrm{d}l, \tag{26}$$

where

$$R_m(r,l) = \int_0^\infty J_0(sr) \frac{s\exp(sc\lambda_m)}{1-\exp(2sc\lambda_m)} \sin(sl)\,\mathrm{d}s, \tag{27}$$

It should be note that Eq. (26) would give the stress and electric displacement for the perturbation problem solved under the conditions (3)–(5). To obtain the correct stress and electric displacement, the solution of the un-cracked medium under prescribed external loads must be added to that given by Eq. (26).

2.5. Crack face electric boundary conditions

Generally, in piezoelectric fracture, two kinds of idealized electrical boundary conditions on the crack faces are extensively used. One commonly boundary condition is the specification that the normal component of electric displacement on the crack surfaces equals zero. This electrical boundary condition ignores the permittivity of the medium inside the crack. Another commonly used boundary condition treats the crack faces as being electrically contacted.

2.5.1. Electrically impermeable cracks

The simplest way to solve the problem is to consider the crack as electrically impermeable and the electric displacement inside the crack is zero. Thus, in Eq. (22) $d_0 = 0$; and Eq. (20) can be solved by using a collocation technique where the functions Φ_j are found at discrete points by matching the discrete values of the nonhomogeneous terms of the integral equations.

2.5.2. Electrically contacted cracks

Section 2.5.1 gives the solution for the electrically impermeable crack face boundary condition. In that extreme case the crack face is free of electric charges and the equivalent crack face electric displacement load is $p_{20} = -D_0$ where D_0 is obtained from the solution of the same medium without cracks. Here we consider another extreme case in which the electric displacement on the crack faces is unknown but the electric potential jump across the upper and lower surfaces of the cracks is zero (i.e., $\Phi_2 = 0$ so that the crack faces are at an electrically contacted state). The only unknown for this problem is Φ_1 which can be determined from the first equation of Eq. (20):

$$\Lambda_{11}^0 \Phi_1(l) + \int_0^a K_{11}(l,r)\Phi_1(r)\,\mathrm{d}r = \frac{2}{\pi}\int_0^l \frac{x p_{01}(x)}{\sqrt{l^2 - x^2}}\,\mathrm{d}x. \tag{28}$$

It can be shown that the applied electric loads have no effect on the solution of the problem. The stress and electric displacement intensity factors are obtained from

$$k_1 = -\frac{1}{\sqrt{a}}\Lambda_{11}\Phi_1(a), \qquad k_{\mathrm{D}} = \frac{\Lambda_{21}}{\Lambda_{11}}k_1. \tag{29}$$

The displacement on the upper surfaces of the electrically contacted cracks is the same as the first of Eq. (25). For an electrically contacted crack, the electric potential jump across the cracks is zero and the electric charges will be accumulated on the crack surfaces. The electric displacement on the crack faces d_0 can be obtained from the second of Eq. (20). It follows that d_0 satisfies the equation

$$\Lambda_{21}^0 \Phi_1(l) + \int_0^a K_{21}(l,r)\Phi_1(r)\,\mathrm{d}r = \frac{2}{\pi}\int_0^l \frac{x p_{02}(x)}{\sqrt{l^2 - x^2}}\,\mathrm{d}x, \tag{30}$$

where $p_{02} = d_0 - D_0$. Eq. (30) is an Abel type integral equation. With its solution we obtain:

$$d_0(x) = D_0(x) + \frac{1}{x}\frac{\mathrm{d}}{\mathrm{d}x}\int_0^x \frac{t}{\sqrt{x^2 - t^2}}\left[\Lambda_{21}^0\Phi_1(t) + \int_0^a K_{21}(t,r)\Phi_1(r)\,\mathrm{d}r\right]\mathrm{d}t. \tag{31}$$

The electric displacement inside the crack d_0 consists of two parts. The first part is the first term on the right-hand-side of Eq. (31), which is equal to the applied electric displacement load D_0. The second part is the second term on the right-hand-side of Eq. (31), which is produced by the applied mechanical load σ_0 on the crack faces.

3. Numerical results and discussion

In this section, some sample results are given for a PZT-4 piezoelectric ceramic. Material properties are (Giannakopoulos and Suresh, 1999): $c_{11} = 139$ GPa, $c_{13} = 74.3$ GPa, $c_{33} = 115$ GPa, $c_{44} = 25.6$ GPa, $c_{12} = 77.8$ GPa, $e_{31} = -5.2$ C/m^2, $e_{33} = 15.1$ C/m^2, $e_{15} = 12.7$ C/m^2, $\epsilon_{11} = 64.61 \times 10^{-10}$ F/m, and $\epsilon_{33} = 56.2 \times 10^{-10}$ F/m. The temperature–stress coefficients are denoted as λ_{11} and λ_{33}, and the temperature–electric displacement coefficient is denoted as β_3. In the following Sections 3.1–3.3, a constant stress load $\sigma_{zz}(r,\infty) = \sigma_0$, a constant electric displacement load $D_z(r,\infty) = D_0$, and a transient heating on the outer surface of a cylinder are considered, separately.

3.1. A constant axial stress load $\sigma_{zz}(r,\infty) = \sigma_0$ applied at infinity

Fig. 2 gives the normalized stress intensity factors with crack spacing. Electrically impermeable crack and electrically contacted crack solutions are plotted. To explore the effect of piezoelectric coefficients,

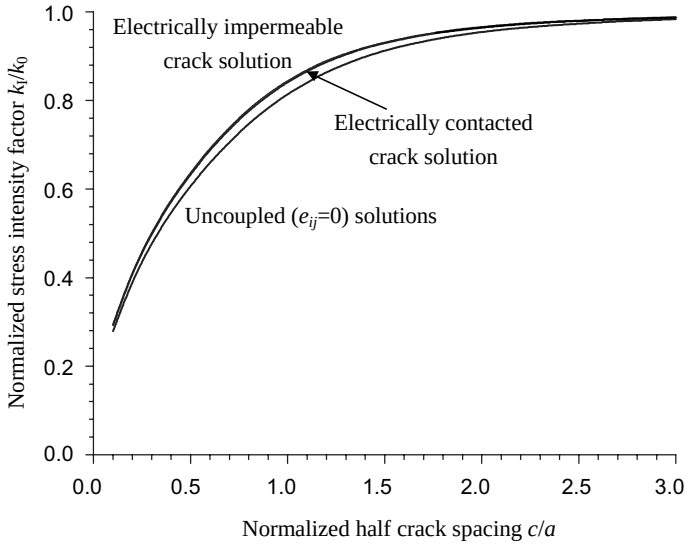

Fig. 2. Stress intensity factors produced by a far-field constant stress load σ_0. ($k_0 = \frac{2}{\pi}\sigma_0\sqrt{a}$).

the un-coupled solutions (i.e. solution for $e_{ij} = 0$) are also displayed. Obviously, the crack face electric boundary condition assumptions have little influence on k_1. However, the effect of piezoelectric coefficients on the stress intensity factor is not neglectable. Such a fact suggests that the stress intensity factors for traditional materials may not be directly used to the piezoelectric materials and fully coupled analysis is required. For relatively large values of crack spacing (i.e. for large values of c/a) the effect of piezoelectric effect is not pronounced. Moreover, the results indicate that multiple cracking has a significant tendency to release the stress intensity factors. In each case, the normalized value of k_1 decreases monotonously with decreasing crack spacing from unit to zero.

Depicted in Fig. 3 are the stress $\sigma_{zz}(0, c)$ for different values of c/a. Once again, the electrically contacted crack assumption and the electrically impermeable crack assumption almost give the same stress prediction. However, the effect of piezoelectric coefficients on the stresses is very significant. Unlike the stress intensity factor, the dependency of the stress on the crack spacing is more complicated. It can be shown that there exists a maximum value of the stress, which multiple cracking can release. The value of

$$\sigma_{\min}(0, c) = 0.2\sigma_0 \tag{32}$$

in the periodically cracked medium is achieve when $c \approx 0.5a$.

Some additional results for the electric displacement intensity factors and electric displacements are given in Figs. 4 and 5, respectively. Both k_D and D_z strongly depend on the crack face electric boundary condition assumptions, especially for small values of crack spacing. Note that in the case of electrically contacted cracks the electric displacement intensity factors can related to the stress intensity factor solution through Eq. (29), which for the present material, is

$$k_D = 2.501 \times 10^{-10} k_1. \tag{33}$$

For a single crack in the medium, the electric displacements on the crack faces are zero which do not depend on the crack fact electric boundary conditions. k_D for a single impermeable crack is also zero. These facts suggest that the stress and electric displacement are only un-coupled at cracked plane ahead of the crack front when the cracks are infinitesimal and are sufficiently largely spaced.

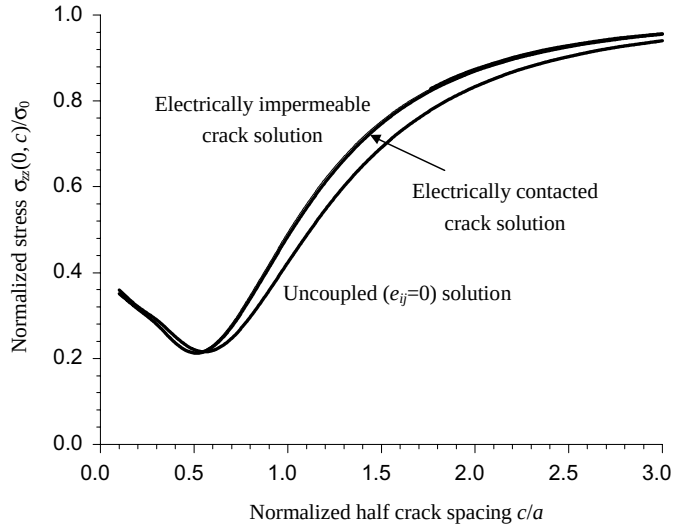

Fig. 3. Stresses produced by a far-field constant stress load σ_0.

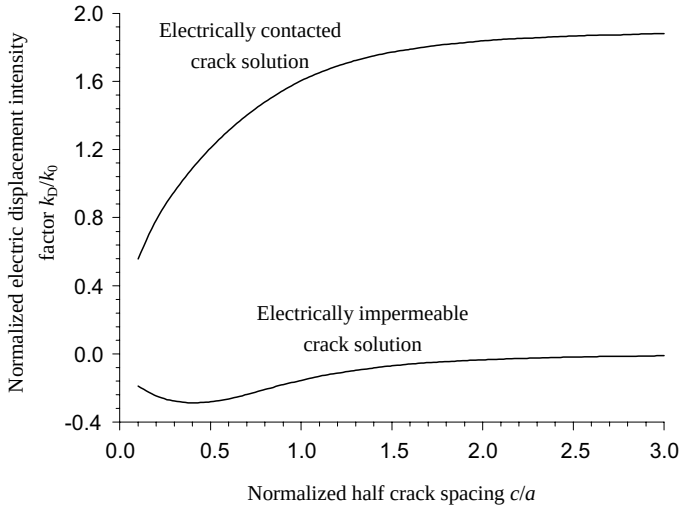

Fig. 4. Electric displacement intensity factors produced by a far-field constant stress load σ_0. ($k_0 = \frac{2}{\pi}\frac{e_{33}}{c_{33}}\sigma_0\sqrt{a}$).

3.2. A constant axial electric displacement load $D_z(r, \infty) = D_0$ applied at infinity

Figs. 2–5 are solutions for a constant mechanical load σ_0. In most cases, the electrical load and mechanical load are applied simultaneously. Since the electrically contacted cracks do not obstruct any electric fields, field intensity factors are zero for electrically contacted cracks under electric loads. Therefore, only the impermeable crack solutions need to be considered. Figs. 6 and 7 give the stresses and stress intensity factors, and the electric displacements and the electric displacement intensity factors, respectively, for an applied electrical displacement load D_0. Explanations for the effect of the crack spacing on the intensity factors are similar to the mechanical load case. Based on the analytical results, it is possible to show that

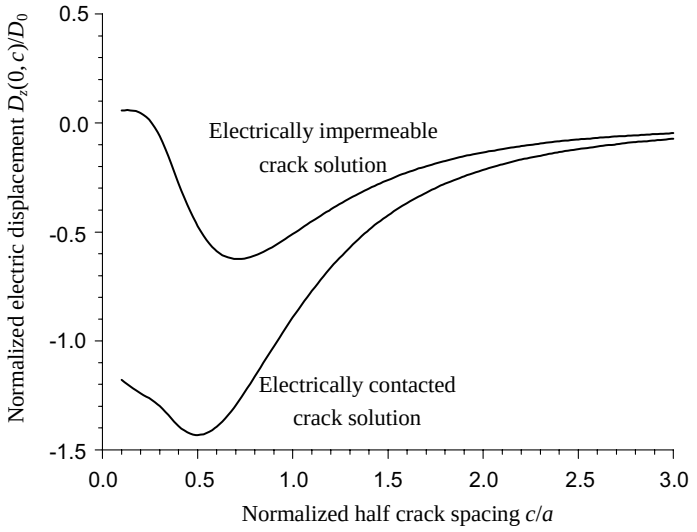

Fig. 5. Electric displacements produced by a far-field constant stress load σ_0. ($D_0 = \frac{e_{33}}{c_{33}}\sigma_0$).

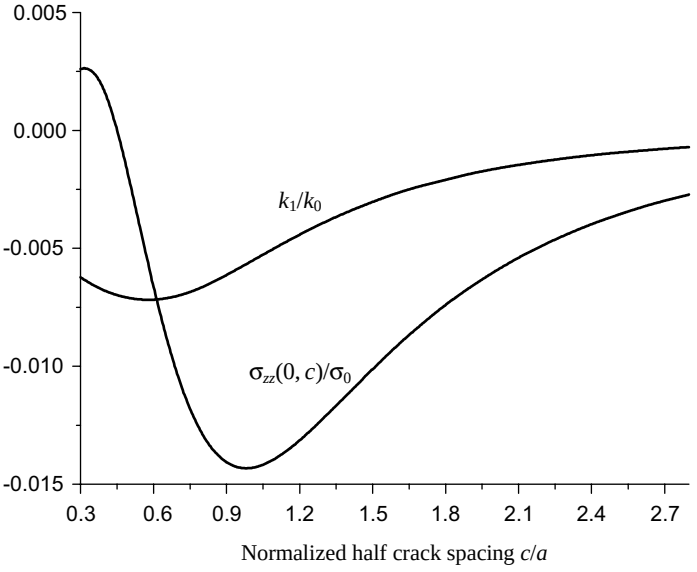

Fig. 6. Stresses and stress intensity factors produced by a far-field constant electric displacement load D_0. ($\sigma_0 = \frac{e_{33}}{c_{33}}D_0$; $k_0 = \frac{2}{\pi}\frac{e_{33}}{\epsilon_{33}}D_0\sqrt{a}$).

the applied electrical load can only produce very small stress and stress intensity factor. We discuss this quantitatively in the following.

If the applied stress and electric field are prescribed, the equivalent electric displacement load can be obtained from

$$D_0 = \frac{c_{11}e_{33} - c_{13}e_{31}}{c_{11}c_{33} - c_{13}^2}\sigma_0 + \left[\epsilon_{33} + \frac{c_{11}e_{33}^2 - 2c_{13}e_{31}e_{33} + c_{33}e_{31}^2}{c_{11}c_{33} - c_{13}^2}\right]E_0, \tag{34}$$

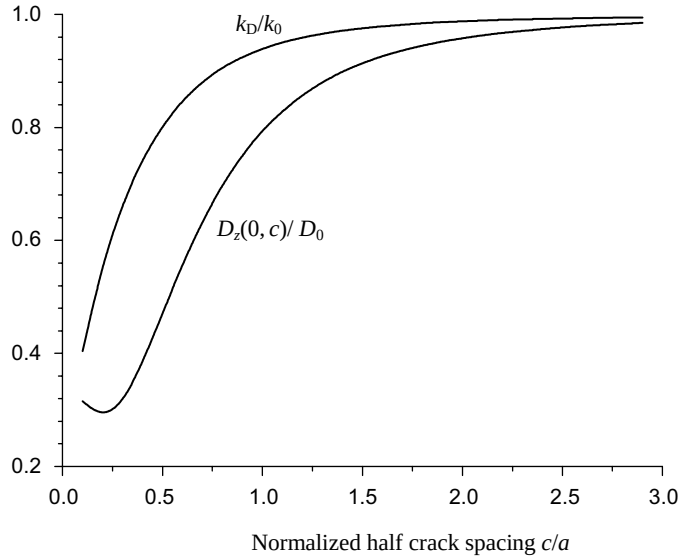

Fig. 7. Electric displacements and electric displacement intensity factors produced by a far-field constant electric displacement load D_0. ($k_0 = \frac{2}{\pi} D_0\sqrt{a}$).

which is $(2.345\sigma_0 + 100.61E_0) \times 10^{-10}$ C/m^2 for the present piezoelectric ceramic. Suppose there is a sufficiently large electric field $E = 1$ MV/m applied along the negative z direction on the medium, then the maximum stress produced by this electric field can be found from the results in Fig. 6. It can be shown that the maximum stress and stress intensity factor

$$\sigma_{\max} \approx 0.0144 \times \frac{15.1}{56.2} \times 100.61 \times 10^6 \approx 0.4 \text{ MPa} \tag{35a}$$

and

$$k_{1\max} \approx 0.00722 \times \frac{2}{\pi} \times \frac{15.1}{56.2} \times 100.61 \times 10^6 \sqrt{a} \approx 0.124 \text{ MPa}\sqrt{\text{a}}, \tag{35b}$$

appear approximately at $c/a = 1$ and $c/a = 0.58$, respectively. Comparing with the strength limit and the fracture toughness of the common materials, these values are not significant. (Note that for a sufficient large crack radius, say, for example, $a = 1$ cm, Eq. (35b) gives $k_{1\max} \approx 0.0124$ MPa$\sqrt{\text{m}}$, which is a very small value.)

3.3. A transient heating on the outer surface of a piezoelectric cylinder

The problem considered in this subsection is a piezoelectric cylinder described in Fig. 8. The z-axis is oriented in the poling direction of the piezoelectric medium. The cylinder has a radius b and is infinite along its axial direction. Suppose the piezoelectric medium is initially at a uniform temperature zero, and its outer surface undergoes a sudden temperature variation T_0. That is

$$T(r,0) = 0, \qquad T(b,t) = T_0 H(t), \tag{36}$$

which defines a thermal shock condition on the outer surface of the medium where $H(t)$ is the Heaviside function. Since the external temperature is only a function of the radial coordinate r and the time variable

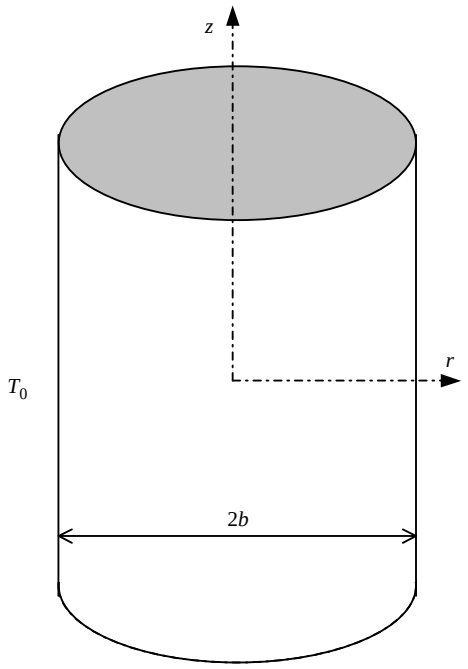

Fig. 8. A piezoelectric cylinder subjected to a sudden heating on its outer surface.

t, the heat conduction is also one-dimensional along the r direction. For such a one-dimension heat conduction, the temperature field T can be found from thermal stress textbook as

$$T(r,t) = T_0 - T_0 \sum_{m=1}^{\infty} \frac{2}{\gamma_n J_1(\gamma_n)} J_0\left(\gamma_n \frac{r}{b}\right) \exp\left(-\gamma_n^2 \frac{t}{t_0}\right), \tag{37}$$

where $t_0 = \rho c_v b^2/k_2$, $J_i\,(i = 1, 2)$ are the ith Bessel functions of the first kind, and γ_n are the roots of the equation $J_0(\gamma) = 0$, k_2 is the coefficient of thermal conductivity of the medium in the radial direction, ρ the density, and c_v the specific heat. It can be seen immediately that the thermal diffusivity $k_2/\rho c_v$ dictates the time scale for transient temperature distribution, but does not affect the level of the temperature.

3.3.1. Electro-elasticity fields in the piezoelectric medium in the absence of cracks

From the overall equilibrium of the cylinder, the total force and electric charge along the axial direction should be zero. The axial thermal stress σ_0 and the axial electric displacement D_0 can be obtained as

$$\begin{Bmatrix} \sigma_0(r,t) \\ D_0(r,t) \end{Bmatrix} = -\begin{Bmatrix} \bar{\lambda}_{33} \\ \bar{\beta}_3 \end{Bmatrix} T_0 \sum_{m=1}^{\infty} \left[\frac{4}{\gamma_n^2} - \frac{2}{\gamma_n J_1(\gamma_n)} J_0\left(\gamma_n \frac{r}{b}\right)\right] \exp\left(-\gamma_n^2 \frac{t}{t_0}\right), \tag{38}$$

where

$$\bar{\lambda}_{33} = \lambda_{33} - \frac{c_{13}}{c_{11}}\lambda_{11}, \qquad \bar{\beta}_3 = \beta_3 - \frac{e_{31}}{c_{11}}\lambda_{11}, \tag{39}$$

hereafter c_{ij}, e_{ij} and ϵ_{ii} are elastic constants, piezoelectric constants and dielectric permittivities, respectively; λ_{ii} are the temperature–stress coefficients; β_3 is the temperature–electric displacement coefficient; T is the temperature change in the medium.

Eq. (38) indicate that among many thermo-electro-mechanical parameters in the piezoelectric materials, the parameters that govern the transient thermal stress and electric displacement levels in the cylinder are identified as $\bar{\lambda}_{33}$ and $\bar{\beta}_3$. The time scale for the transient thermal stress and electric displacement state is governed by the thermal diffusivity $\rho c_v/k_2$, which does not affect the levels of thermal stresses and electric displacements.

The evaluation of the dimensionless thermal stresses and electric displacements are plotted against the dimensionless Fourier number $F_0 = t/t_0$, where $t_0 = \rho c_v b^2/k_2$, in Fig. 9 for different positions in the cylinder. For any given position in the cylinder, the transient thermally induced electro-mechanical field is zero initially, increases to a peak as time goes on, and then decreases to zero as time approaches infinity. It is clear that if $T_0 > 0$, the region near the surface of the cylinder experience a compressive stress while a tensile zone is developed at the center of the cylinder. The maximum compressive stress is attained at the surface and the tensile stress is largest at the center of the cylinder. The maximum values of

$$\sigma_0 = -\bar{\lambda}_{33} T_0, \qquad D_0 = -\bar{\beta}_3 T_0 \tag{40a}$$

are achieved at the surface of the cylinder at $t = 0$. The maximum tensile stress and the electric displacement

$$\sigma_0 = 0.471 \bar{\lambda}_{33} T_0, \qquad D_0 = 0.471 \bar{\beta}_3 T_0 \tag{40b}$$

are attained at the center of the cylinder at a time $t/t_0 = 0.0761$. These expressions are valid for any of the piezoelectric materials.

Under a cooling condition ($T_0 < 0$), at any location of the cylinder, the stress and electric displacement will change their signs from the heating condition. Hence the surface of the cylinder will become tensile and the center will be compressive. The magnitudes of the thermal stresses and electric displacements subjected to a cooling will be the same as those in a heating condition.

3.3.2. Field intensity factors, stresses in the cracked cylinder

Since the above analysis shows that under the heating condition, the cylinder has the largest axial tensile stress at its center, while the axial stress at its outer surface is compressive, it is then expected that a row of

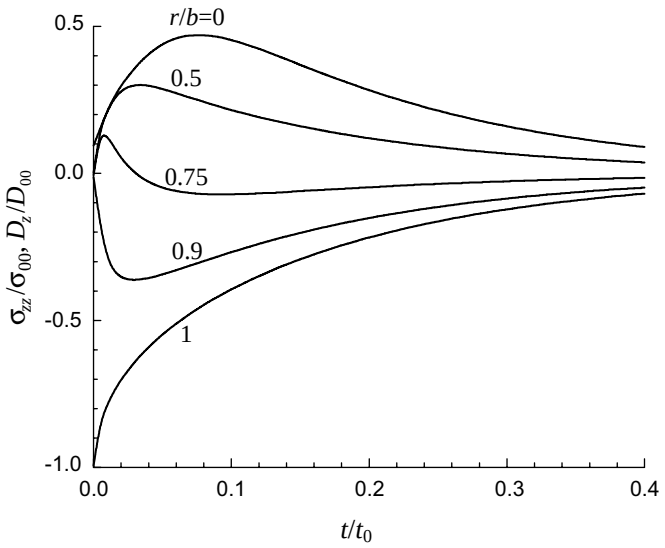

Fig. 9. Distribution of the axial thermal stress $\sigma_0(r,t)$ and electric displacement $D_0(r,t)$ at selected locations r/b. ($\sigma_{00} = \bar{\lambda}_{33} T_0$, $D_{00} = \bar{\beta}_3 T_0$).

infinitesimal cracks may initiate at the center of the cylinder under the heating condition (since we are interested in crack initiation behavior, the assumption of infinitesimal cracks are reasonable). Cracks grow unstably until they enter the compressive region. The problem can be synthesized from the general solution for a row of embedded cracks in a cylinder, with crack fronts located at $r = a$, as shown in Fig. 1. Since the crack planes are normal to the outer surfaces of the cylinder, they do not perturb the transient temperature distribution in this arrangement, determination of the temperature distribution and the resulting thermal stresses and electric displacements for the un-cracked medium would be quite straightforward. The stress and electric displacement given by Eq. (38), with opposite signs, are added to the crack surface mechanical and electrical loads in the quasi-static problem. The problem will then be solved with the general electromechanical model developed in Section 2.

Equivalent crack face applied loads

Since l/b is small, the function $\sin(\gamma_{n\,1}/b)$ equals $\gamma_{n\,1}/b$. It follows from Eqs. (38) and (22) that:

$$Q_1(l) = -\frac{2}{\pi}\int_0^l \frac{r\sigma_0(r,t)}{\sqrt{l^2-r^2}}\,\mathrm{d}r = \bar{\lambda}_{33}T_0 l f(t), \tag{41a}$$

$$Q_2(l) = \frac{2}{\pi}\int_0^l \frac{rd_0(r,t)}{\sqrt{l^2-r^2}}\,\mathrm{d}r - \frac{2}{\pi}\int_0^l \frac{rD_0(r,t)}{\sqrt{l^2-r^2}}\,\mathrm{d}r = \frac{2}{\pi}\int_0^l \frac{rd_0(r,t)}{\sqrt{l^2-r^2}}\,\mathrm{d}r + \bar{\beta}_{33}T_0 l f(t), \tag{41b}$$

where

$$f(t) = \frac{4}{\pi}\sum_{m=1}^{\infty}\frac{1}{\gamma_n^2}\exp\left(-\gamma_n^2\frac{t}{t_0}\right)\left[2 - \frac{1}{J_1(\gamma_n)}\gamma_n\right], \tag{42}$$

is a function of time t and is independent of material properties. Note that in the problem under consideration time t enters into the analysis through $Q_i(l)$ only. The function $f(t)$ is negative for all values of t. Its maximum absolute value is

$$f_{\max} = 0.3, \tag{43}$$

which is attained at the time $t/t_0 = 0.0761$. Once Q_i are obtained, the integral Eq. (20) can be solved and the stress and electric displacement intensity factors can be calculated from Eq. (24), and the stress and electric displacement at the $z = c$ plane can be calculated from Eq. (26).

Stress and stress intensity factors

As pointed out in Sections 3.1 and 3.2, the stress intensity factor k_1 caused by an electric displacement load is negligible. Further, the values of k_1 are almost identical for electrically impermeable cracks and for electrically contacted cracks. Therefore, only thermally induced stress load needs to be investigated.

In Fig. 10, the normalized stress intensity factors $\bar{k} = k_1/k_0$, where $k_0 = (2/\pi)\bar{\lambda}_{33}T_0\sqrt{a}$, are plotted against the dimensionless time t/t_0, for selected normalized crack spacing c/a, where a is the crack radius. At any given c/a, the stress intensity factor increases from an initial zero value with time, displays a peak value and then decreases to zero as time approaches infinity. This means that the thermal stress intensity factors occur only at transient state and that their steady values are zero. The peak values for all values of the crack spacing appear at a same time $t/t_0 = 0.0761$. Further, multiple cracking has a tendency to reduce the transient thermal stress intensity factors. It is interesting to note that when $c/a = 0.25$, the stress intensity factor $k_{1\max} = 0.218k_0$; a value which is 47% of the maximum stress intensity factor for a single isolated crack in infinite media, which is $k_{1\max} = 0.470k_0$.

Fig. 11 displays the normalized thermal stress σ_{zz} at the center of the piezoelectric cylinder (i.e. at $(r,z) = (0,c)$). For each given crack spacing, σ_{zz} has a peak value, which appear at $t/t_0 = 0.0761$. Once again, increasing crack density reduces the thermal stress level considerably. Note that when $c/a = 0.5$, the stress $\sigma_{\max} = 0.0974\sigma_0$; a value which is only 21% of the maximum stress for a single isolated crack in infinite media, which is $\sigma_{\max} = 0.470\sigma_0$.

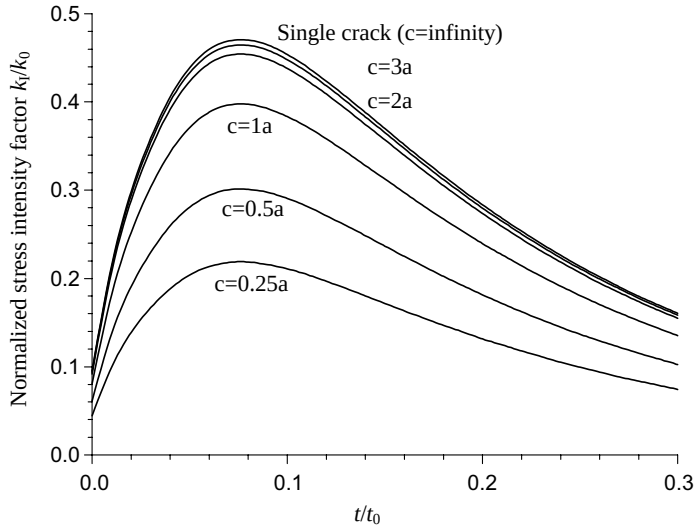

Fig. 10. Stress intensity factors caused by the thermal stress load as a function of time. ($k_0 = (2/\pi)\bar{\lambda}_{33}T_0\sqrt{a}$).

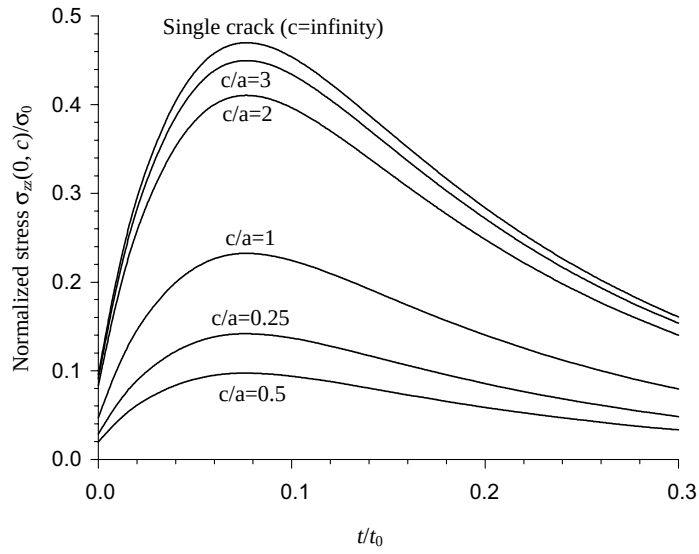

Fig. 11. Stress $\sigma_{zz}(0,c)$ caused by the thermal stress load as a function of time ($\sigma_0 = \bar{\lambda}_{33}T_0$).

Finally, Fig. 12 plots the peak values of the stresses and the stress intensity factors for different crack spacing. As pointed out above, these peak values appear at the same time $t/t_0 = 0.0761$.

3.3.3. Thermal shock resistance studied from the piezoelectric cylinder specimen

Thermal shock represents a rapid temperature change in a medium. Thermal shock resistance is a major issue in the design of engineering ceramics for thermal applications. In evaluation the thermal shock resistance of engineering materials, two criteria are usually used: (i) maximum local tensile stress equals

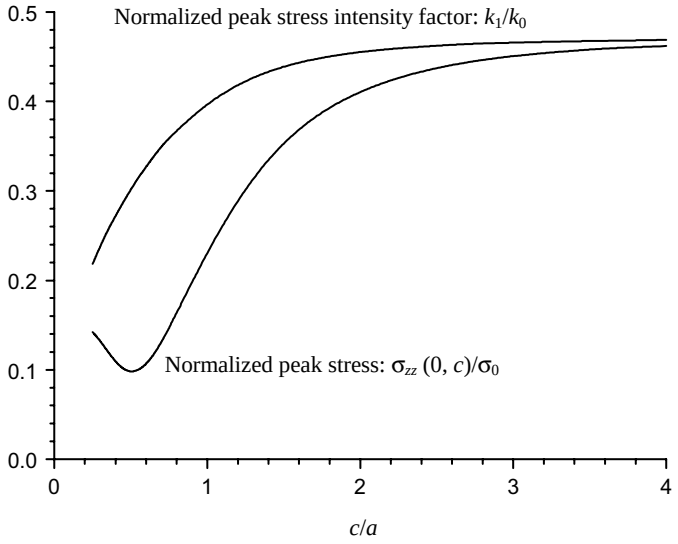

Fig. 12. The peak values of the stress and the stress intensity factor, which appear at $t = 0.0761t_0$ ($\sigma_0 = \bar{\lambda}_{33}T_0$; $k_0 = (2/\pi)\bar{\lambda}_{33}T_0\sqrt{a}$).

the tensile strength of the ceramic, and (ii) maximum stress intensity factor equals the fracture toughness of the ceramic.

From the numerical results in Fig. 12 we know that when there is only a single crack (i.e. c is infinity), the maximum stress and stress intensity factor in the piezoelectric cylinder are

$$\sigma_{\max} = 0.470\bar{\lambda}_{33}T_0 \quad \text{and} \quad k_1 = 0.470(2/\pi)\bar{\lambda}_{33}T_0\sqrt{a}, \tag{44}$$

respectively. For multiple cracking, the stress and stress intensity are less severe. Therefore, failure prediction made from Eq. (44) is conservative.

A stress-based failure criterion for thermal shock is that the maximum thermal stress that appears on the center of the cylinder $\sigma_{\max}$ attains the value σ_b, which is the strength limit of the piezoelectric medium. The maximum temperature jump sustainable by T_c follows from the first of Eq. (44) as

$$T_c = T_c^{\text{stress}} = 2.13\frac{\sigma_b}{\bar{\lambda}_{33}}. \tag{45}$$

Eq. (45) represents the minimum temperature jump sustainable by the medium based on the stress–failure criterion. T_c does not depend on the crack size, and are valid for all materials.

As pointed above, the stress intensity factors for the electrically impermeable cracks and the electrically contacted cracks are same. Therefore, if the stress intensity factor is used as a failure criterion for piezoelectric ceramics, there is no need to consider the electrical boundary conditions on the crack faces. For the fracture-based failure criterion, the maximum thermal stress intensity factor $k_{\max}$ must equal the fracture toughness of the ceramic k_{1c}. From the second of Eq. (44) we know that

$$T_c = T_c^{\text{fracture}} = 3.34\frac{k_{1c}}{\bar{\lambda}_{33}\sqrt{a}}. \tag{46}$$

Eq. (46) represents the minimum temperature jump sustainable by the medium based on the fracture–failure criterion. Clearly, T_c has a strong dependency on the crack radius. T_c decreases as a increases.

Consideration of Eqs. (45) and (46) reveals that the admissible temperature jump is less for fracture–controlled failure than for stress–controlled failure, at a sufficiently large crack radius. A transient crack

size a_t exists for which T_c is equal for fracture-based failure and stress-based failure. Then, upon equating T_c values for the stress-based criterion (45) and for the fracture-based criterion (46), it is found that

$$a_t \approx 2.5\left(\frac{K_{1c}}{\sigma_b}\right)^2. \tag{47}$$

Eq. (47) indicates that a piezoelectric material with crack size a_t has the same thermal strength according to the stress criterion and the fracture criterion. The fracture-based criterion is conservative for cracks sized above a_t, the stress-based criterion is conservative for cracks sized below a_t.

4. Conclusions

This paper focused on the analysis of stress and intensity release by multiple cracks in piezoelectric media subjected to electromechanical and/or transient thermal loading conditions. The poling direction of the piezoelectric plate is perpendicular to the crack planes. An electro-mechanical model is developed for the interactions of a row of cracks periodically located in a piezoelectric material cylinder.

The crack face electrical boundary conditions have little influence on the stress intensity factors, whereas the effect of piezoelectric coupling coefficients (e_{ij}) is essential for multiple cracking.

The magnitude of the transient thermal stress in the cracked medium depends on a number of parameters. Among these parameters, the thermal stresses and the thermal electric displacements in an un-cracked piezoelectric plate are only controlled, respectively, by equivalent parameters $\bar{\lambda}_{33}$ and $\bar{\beta}_3$, which are defined in Eq. (39). The maximum stresses and electric displacements are, respectively, $\sigma_0 = -\bar{\lambda}_{33}T_0$ and $D_0 = -\bar{\beta}_3 T_0$, at the outer surface of the cylinder, and $\sigma_0 = 0.471\bar{\lambda}_{33}T_0$ and $D_0 = 0.471\bar{\beta}_3 T_0$ at the center of the cylinder.

The stresses and stress intensity factors can be released considerably by multiple cracking. Thermally induced stress and electric fields, and the associated thermal fracture mechanics problem for a piezoelectric cylindrical specimen have been obtained theoretically for a periodic array of embedded circular cracks. A transient crack radius a_t is obtained for which the admissible temperature jump is equal for fracture-based criterion and stress-based criterion. The admissible temperature of a piezoelectric ceramic cylinder with cracks smaller than a_t should be evaluate by the stress-based criterion, a cylinder with cracks larger than a_t should be evaluated by the fracture-based criterion.

Acknowledgment

The authors thank the NSFC for supporting their research.

Appendix A

Material constants $C_{jm}(j = 1,\ldots,5;\ m = 1,2,3)$ are as follows:

$$C_{1m} = c_{13}a_{1m} + c_{33}\lambda_m a_{2m} + e_{33}\lambda_m a_{3m}, \tag{A.1}$$

$$C_{2m} = e_{31}a_{1m} + e_{33}\lambda_m a_{2m} - \epsilon_{33}\lambda_m a_{3m}, \tag{A.2}$$

$$C_{3m} = c_{44}\lambda_m a_{1m} - c_{44}a_{2m} - e_{15}a_{3m}, \tag{A.3}$$

$$C_{4m} = c_{11}a_{1m} + c_{13}\lambda_m a_{2m} + e_{31}\lambda_m a_{3m}, \tag{A.4}$$

$$C_{5m} = e_{15}\lambda_m a_{1m} - e_{15}a_{2m} + \epsilon_{11}a_{3m}. \tag{A.5}$$

These coefficients have the relationship:

$$C_{1(3+i)} = C_{1i}, \quad C_{2(3+i)} = C_{2i}, \quad C_{3(3+i)} = -C_{3i}, \quad C_{4(3+i)} = C_{4i}, \quad C_{5(3+i)} = -C_{5i} \qquad (i = 1, 2, 3). \tag{A.6}$$

Appendix B

Integrate the left-hand-side of Eq. (17) by part, we obtain

$$\int_0^a s \sin(sl)\Phi_j(l)\,\mathrm{d}l = -\cos(sa)\Phi_j(a) + \int_0^a \cos(sl)\frac{\mathrm{d}\Phi_j(l)}{\mathrm{d}l}\,\mathrm{d}l. \tag{B.1}$$

Substituting Eq. (B.1) into Eq. (17) and using the integral identity (Gradshteyn and Ryzhik, 1965):

$$\int_0^\infty \cos(sl)J_0(sx)\,\mathrm{d}s = \begin{cases} \dfrac{1}{\sqrt{x^2 - l^2}}, & x > l, \\ 0, & x < l, \end{cases} \tag{B.2}$$

we obtain

$$\sum_{j=1}^{2} \Lambda_{ij}^0 \int_0^x \left[\frac{1}{\sqrt{x^2 - l^2}}\frac{\mathrm{d}\Phi_j(l)}{\mathrm{d}l}\right]\mathrm{d}l + \int_0^a \psi_{ij}(x, r)\Phi_j(r)\,\mathrm{d}r = p_{0i}(x). \tag{B.3}$$

It is well known that the Abel integral equation:

$$f(x) = \int_0^x \frac{g(l)}{\sqrt{x^2 - l^2}}\,\mathrm{d}l, \tag{B.4}$$

has a solution:

$$g(l) = \frac{2}{\pi}\frac{\mathrm{d}}{\mathrm{d}l}\int_0^l \frac{xf(x)}{\sqrt{l^2 - x^2}}\,\mathrm{d}x. \tag{B.5}$$

Hence, it can be shown from Eq. (B.3) that

$$\sum_{j=1}^{2} \Lambda_{ij}^0 \Phi_j(l) + \frac{2}{\pi}\int 0^l \frac{x\int_0^a \sum_{j=1}^{2}\psi_{ij}(x, r)\Phi_j(r)\,\mathrm{d}r}{\sqrt{l^2 - x^2}}\,\mathrm{d}x = \frac{2}{\pi}\int_0^l \frac{xp_{0i}(x)}{\sqrt{l^2 - x^2}}\,\mathrm{d}x. \tag{B.6}$$

By substituting Eq. (19) into Eq. (B.6), and using the result

$$\int_0^l \frac{xJ_0(sx)}{\sqrt{l^2 - x^2}}\,\mathrm{d}x = l\int_0^1 \frac{mJ_0(sml)}{\sqrt{1 - m^2}}\,\mathrm{d}m = \frac{\sin(sl)}{s}, \tag{B.7}$$

Eq. (20) is obtained.

References

Erdogan, F., Ozturk, M., 1995. Periodic cracking of functionally graded coatings. Int. J. Eng. Sci. 33, 2179–2195.

Gao, C.F., Zhao, Y.T., Wang, M.Z., 2002. An exact and explicit treatment of an elliptic hole problem in thermopiezoelectric media. Int. J. Solids Struct. 39, 2665–2685.

Gao, C.F., Tong, P., Zhang, T.Y., 2004. Fracture mechanics for a mode III crack in a magnetoelectroelastic solid. Int. J. Solids Struct. 41, 6613–6629.

Giannakopoulos, A.F., Suresh, S., 1999. Theory of indentation of piezoelectric materials. Acta Mater. 47 (7), 2153–2164.

Gradshteyn, I.S., Ryzhik, I.M., 1965. Tables of Integrals, Series and Products. Academic Press, New York.

Grot, A.S., Martyn, J.K., 1981. Behavior plasma-sprayed ceramic thermal barrier coating for gas turbine engines. Bull. Am. Cer. Soc. 60, 807–811.

Gu, B., Yu, S.W., 2003. The thermal effect of piezoelectric medium for anti-plane problem under high electrical impact loading. Comput. Mater. Sci. 28, 628–632.

Herrmann, K.P., Loboda, V.V., 2003a. Fracture mechanical assessment of interface cracks with contact zones in piezoelectric bimaterials under thermoelectromechanical loadings I. Electrically permeable interface cracks. Int. J. Solids Struct. 40, 4191–4217.

Herrmann, K.P., Loboda, V.V., 2003b. Fracture mechanical assessment of interface cracks with contact zones in piezoelectric bimaterials under thermoelectromechanical loadings II. Electrically impermeable interface cracks. Int. J. Solids Struct. 40, 4219–4237.

Ishihara, M., Noda, N., 2001. A piezoelectric-elastic body with inhomogeneities and a crack under plane electrical and anti-plane mechanical loads. Arch. Appl. Mech. 71, 577–588.

Lin, S., Narita, F., Shindo, Y., 2003. Electroelastic analysis of a piezoelectric cylindrical fiber with a penny-shaped crack embedded in a matrix. Int. J. Solids Struct. 40, 5157–5174.

Lu, P., Tan, M.J., Liew, K.M., 1998. Piezothermoelastic analysis of a piezoelectric material with an elliptic cavity under uniform heat flow. Arch. Appl. Mech. 68, 719–733.

Niraula, O.P., Noda, N., 2002. Thermal stress analysis in thermopiezoelastic strip with an edge crack. J. Therm. Stresses 25, 389–405.

Qin, Q., Mai, Y., 1999. A closed crack tip model for interface cracks in thermopiezoelectric materials. Int. J. Solids Struct. 36, 2463–2479.

Rizk, Abd El-Fattah, 2004. Periodic array of cracks in a strip subjected to surface heating. Int. J. Solids Struct. 41, 4685–4696.

Schulze, G.W., Erdogan, F., 1998. Periodic cracking of elastic coatings. Int. J. Solids Struct. 35, 3615–3634.

Shang, F., Kitamura, T., Kuna, M., 2003. Theoretical investigation of an elliptical crack in thermopiezoelectric material. Part II: Crack propagation. Theor. Appl. Fract. Mech. 40, 247–253.

Timm, D.H., Guzina, B.B., Voller, V.R., 2003. Prediction of thermal crack spacing. Int. J. Solids Struct. 40, 125–142.

Ueda, S., 2003. Thermally induced fracture of a piezoelectric laminate with a crack normal to interfaces. J. Therm. Stresses 26, 311–331.

Wang, B.L., Mai, Y.-W., 2003. Thermal shock fracture of piezoelectric materials. Philos. Mag. A 83, 631–657.

Wang, B.L., Noda, N., 2004. Exact thermo-electro-elasticity solution for a penny-shaped crack in piezoelectric materials. J. Therm. Stresses 27, 241–251.

Zhang, T.Y., Zhao, M.H., Tong, P., 2002. Fracture of piezoelectric ceramics. Adv. Appl. Mech. 38, 147–289.